Multifield Methods for Nuclear Thermalhydraulics Problems

S. Banerjee
Department of Chemical and Nuclear Engineering
University of California
Santa Barbara, CA 93106

Abstract
The multifield model, in which separate sets of conservation equations are written for each phase, or clearly identifiable portion of a phase, is derived by averaging the local instantaneous equations. The closure relationships required to replace information lost in the averaging process are discussed. The mathematical structure of the model is considered and it is shown that application to a variety of problems in which the phases are well separated leads to good predictions of experimental data. For problems in which the phases are more closely coupled, the model is more difficult to apply correctly. However, careful consideration of interfield momentum and heat transfer is shown to give excellent results for some complex problems like density wave propagation in bubbly flows. The model in its present form is shown to be less useful for highly intermittent regimes like slug and churn flows. Data on a reflux condensation situation near the flooding point are discussed to indicate directions in which further work is required.

Résumé
Le modèle multifluides dans lequel des systèmes separés d'équations de conservation sont écrits pour chaque phase, ou pour chaque portion clairement identifiable d'une phase, est demontré en moyennant les équations locales instantanées. Les relations de fermeture necessaires pour replacer les informations perdues au cours de l'opération de moyenne sont discutées. La structure mathématique du modèle est considerée et il est montré que des applications à des problèmes variés dans lesquels les phases sont bien separées conduits a de bonnes predictions des résultats experimentaux. Pour des problèmes où les phases sont plus fortement couplées, il est plus difficile d'appliquer correctement le modèle. Néanmoins, il est demontré que la considération soigneuse du moment interfluides et du transfer de chaleur donne d'excellents résultats pour des problèmes complexes comme la propagation d'ondes de densité en milieu à bulles. Il est demontré que le modèle dans sa présente forme est moins utile pour des régimes d'écoulements fortement intermittents comme les écoulements à poches ou à bouchons. Quelques résultats expérimentaux, concernant une situation de condensation à reflux, sont presentés pour indiquer les directions vers lesquels un travail plus approfondi est nécessaire.

Introduction

The approach to 2-phase flow modelling that is now widely used in computer codes like TRAC, and RELAP5 [see the TRAC PD2 manual 1982, and Ransom *et al.* 1984] is based on averaging of the original local instantaneous conservation equations for mass, momentum, and energy. Averaging may be done in time, space, over an ensemble, or in some combination of these, and details may be found in Panton (1968); Vernier and Delhaye (1968); Delhaye (1970); Drew (1971); Kocamustafaogullari (1971); Ishii (1971); Boure *et al.* (1975); Ishii (1975); Delhaye and Achard (1976); Hughes *et al.* (1976); Yadigaroglu and Lahey (1976); Agee *et al.* (1978); Lyczkowski *et al.* (1978); Nigmatulin (1978, 1979); Banerjee and Chan (1980); and Drew (1983), amongst others. The procedure is to derive an averaged set of conservation equations for each field. A field may be thought of as a clearly identifiable portion of a phase, e.g., annular flow may be modelled with 3 fields – one for the liquid film, one for the droplets, and one for the gas core. Selection of the fields depends on the modeller but should, in the spirit with which the model is derived, in all cases be consistent with the physics of the problem. To illustrate this point further, a vertical slug flow might be described by 4 fields – the first for the large bullet-shaped gas bubbles, the second for the liquid film around these bubbles, the third for the highly dispersed gas bubbles in between the large gas bubbles, and the fourth for the liquid surrounding the dispersed bubbles. This level of sophistication may be required in some cases for highly intermittent flows.

While averaging makes the mathematical solution of 2-phase flow problems tractable, information regard-

Keywords: multifield methods, thermalhydraulics, loss of coolant, two-phase flow analysis

ing local gradients between fields and the distribution of phases is lost. Therefore, closure relationships or 'constitutive equations' are required to replace this information. Typically, one needs relationships for interfield forces, heat transfer, and area. For problems involving vaporization and condensation of one component, interfield mass transfer may be related to heat transfer, but in more general problems interfield mass transfer relationships are also needed.

Since averaging also eliminates information regarding the distribution of fields, distribution coefficients relating products of averages to averages of products are therefore also needed. By judiciously choosing fields that are relatively homogeneous, the requirement for distribution coefficients may be minimized, but is difficult to eliminate entirely for all flow regimes.

The form of the closure relationships has important consequences for the mathematical structure of the problem and solution procedures. For example, the simplest multifield models which account for interfield forces through algebraic drag correlations invariably result in high-wavenumber instabilities that are not physical [see, for example, Drew (1983), and Ramshaw and Trapp (1978)]. Considerable work has been done to resolve this problem. The main reason for the non-physical behaviour now appears to lie in rather subtle aspects of pressure interactions between fields, aspects that were neglected in the early models. Recent work on these interactions leads to excellent prediction of a variety of phenomena, as will be discussed later in the paper.

We will first outline the derivation of the averaged conservation equations, identify the closure relationships needed, and analyze the mathematical structure of the multifield model. We will then illustrate the application of the model to flows in which the fields are loosely coupled, i.e., separated flows, and then flows in which the fields are more closely coupled. Finally, the difficulties with the model for intermittent flows will be discussed.

The Multifield Model

Averaged Conservation Equations

The local instantaneous form of the conservation equations for phase k may be written as

$$\frac{\partial \rho_k \psi_k}{\partial t} + \nabla\cdot\rho_k\psi_k\vec{V}_k + \nabla\cdot\gamma_k - \rho_k\hat{S}_k = 0, \tag{1}$$

where conservation requires

$$\begin{aligned} &\psi_k = 1,\ \gamma_k = 0,\ \hat{S}_k = 0, \quad \text{for mass,} \\ &\psi_k = \vec{V}_k,\ \gamma_k = p_k\bar{\bar{I}} - \bar{\bar{\tau}}_k,\ \hat{S}_k = \vec{F}_k \quad \text{for momentum, and} \\ &\psi_k = E_k,\ \gamma_k = \vec{q}_k - (p_k\bar{\bar{I}} - \bar{\bar{\tau}}_k)\cdot\vec{V}_k,\ \hat{S}_k = \vec{F}_k\cdot\vec{V}_k + Q_k \\ &\qquad\qquad \text{for energy conservation.} \end{aligned} \tag{2}$$

Here $\vec{V}$ is velocity, p is pressure, $\bar{\bar{\tau}}$ is the shear stress tensor, $E = e + \vec{V}\cdot\vec{V}/2$ is the internal plus kinetic energy, ρ is density, $\bar{\bar{I}}$ is the identity tensor, $\vec{F}$ is body force, Q is the body heat source, and $\vec{q}$ is heat flux.

While these equations, together with appropriate boundary and initial conditions, constitute the exact mathematical problem, they cannot even be solved for high Reynolds single-phase flow. Direct simulation using super-computers is becoming possible for some simple single-phase flow situations, but is still far in the future for flows in which interface motion and configuration are an integral part of the problem. Because the mathematical problem is impossible to solve at present, the governing equations are reduced to solvable forms by a variety of procedures. The procedure that is most widely used is to volume average the equations, and then time / ensemble average them. The averaging operations are commutative and the order can be reversed, resulting in the same averaged equations. Volume averaging is done rather than area averaging, to assure that the dependent variables and their first derivatives are continuous [see Banerjee and Chan (1980) for more detail].

The procedure will be illustrated for volume averaging of two-phase flow in a duct. Consider the flow situation in Figure 1, which defines the symbols. In this case, 2 phases are shown, but the derivation is not affected if there were more than 2 phases or fields. To proceed, forms of Gauss' theorem and Liebnitz's rule particular to this geometry will be used. We will use these relationships to interchange derivative and volume integral operations. They are:

Leibnitz's rule

$$\frac{\partial}{\partial t}\int_{V_k(z,t)} f(x, y, z, t)dV = \int_{V_k}\frac{\partial f}{\partial t}\,dV + \int_{a_i} f(\vec{V}_i\cdot\vec{n}_k)dS; \tag{3}$$

Gauss' theorem

$$\int_{V_k(z,t)}\nabla\cdot\vec{a}dV = \frac{\partial}{\partial z}\int_{V_k}\vec{n}_z\cdot\vec{a}dV + \int_{a_i}\vec{n}_k\cdot\vec{a}\,dS. \tag{4}$$

Defining

$$\langle f_k\rangle = \frac{1}{V_k}\int_{V_k} f_k\,dV$$

and

$$\langle f_k\rangle_i = \frac{1}{V}\int_{a_i} f_k\,dS$$

and

$$\alpha_k = V_k/V,$$

the volume averaged conservation equations are

$$\frac{\partial}{\partial t}\overline{\alpha_k\langle\rho_k\rangle} + \frac{\partial}{\partial z}\overline{\alpha_k\langle\rho_k u_k\rangle} = -\overline{\langle\dot{m}_k\rangle_i} = -\overline{\rho_k\vec{n}_k\cdot(\vec{V}_i - \vec{V}_k)}; \tag{5}$$

$$\begin{aligned} &\frac{\partial}{\partial t}\overline{\alpha_k\langle\rho_k u_k\rangle} + \frac{\partial}{\partial z}\overline{\alpha_k\langle\rho_k u_k^2\rangle} + \frac{\partial}{\partial z}\overline{\alpha_k\langle p_k\rangle} + \frac{\partial}{\partial z}\overline{\alpha_k\langle\vec{n}_z(\bar{\bar{\tau}}_k\cdot\vec{n}_z)\rangle} - \\ &\alpha_k\langle\rho_k\vec{F}_k\rangle = -\frac{1}{V}\int_{a_i}\overline{[\dot{m}_k u_k + \vec{n}_z\cdot\vec{n}_k p_k - \vec{n}_z\cdot(\vec{n}_k\cdot\bar{\bar{\tau}}_k)]}\,dS + \\ &\frac{1}{V}\int_{a_{kw}}\overline{\vec{n}_z\cdot(\vec{n}_{kw}\cdot\bar{\bar{\tau}}_k)}\,dS; \text{ and} \end{aligned} \tag{6}$$

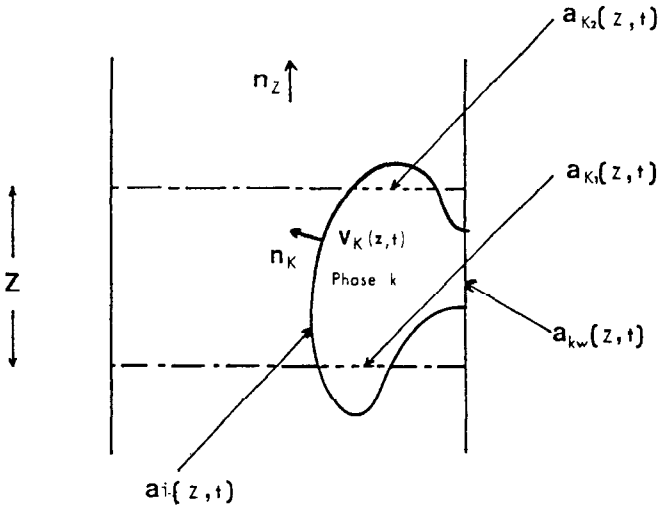

Figure 1 Schematic of two-phase flow field defining the symbols.

$$\frac{\partial}{\partial t}\overline{\alpha_k\langle\rho_k E_k\rangle} + \frac{\partial}{\partial z}\overline{\alpha_k\langle\rho_k u_k E_k\rangle} + \frac{\partial}{\partial z}\overline{\alpha_k\langle\vec{q}_k\cdot\vec{n}_z\rangle} + \frac{\partial}{\partial z}\overline{\alpha_k\langle p_k u_k\rangle} -$$

$$\frac{\partial}{\partial z}\overline{\alpha_k\langle\vec{n}_z\cdot(\bar{\bar{\tau}}_k\cdot\vec{V}_k)\rangle} - \overline{\alpha_k\langle\rho_k(\vec{F}_k\cdot\vec{V}_k + Q_k)\rangle} = -$$

$$\overline{\frac{1}{V}\int_{a_i}[\dot{m}_k E_k + \vec{n}_k\cdot(\vec{q}_k + p_k\vec{V}_k - \bar{\bar{\tau}}_k\cdot\vec{V}_k)]\,dS} -$$

$$\overline{\frac{1}{V}\int_{a_{kw}}\vec{n}_{kw}\cdot q_k\,dS}. \qquad (7)$$

Here $\dot{m}_k$ is the mass transfer out of phase k, and u_k is the velocity in the z direction. The terms involving derivatives of $\bar{\bar{\tau}}$ and $\vec{q}$ on the left hand sides, i.e., axial diffusion of momentum or heat due to molecular effects, are often neglected, since they are very small in most cases. The overbar signs indicate that an ensemble or time averaging operation has been carried out after volume averaging. Double averaging leads to certain desirable properties, which will not be considered further here, but Delhaye and Achard (1978) may be consulted for a definitive discussion.

These equations apply not only to each plane, but to any clearly identified portions of a phase, which is often called a 'field,' provided appropriate relationships are supplied for the quantities on the right-hand side. The central difficulty with such an averaged multifield model arises from all information being lost about the gradients between fields and at the wall. Therefore, closure relationships must be supplied for all the integrals on the right-hand sides, since they cannot be calculated *a priori* from the model. This happens as well in single-phase flow, where the momentum equation is often phrased as

$$\frac{\partial}{\partial t}\overline{\langle\rho u\rangle} + \frac{\partial}{\partial z}\overline{\langle\rho u^2\rangle} + \overline{\frac{\partial\langle p\rangle}{\partial z}} = \overline{\frac{1}{V}\int_{a_{kw}}\vec{n}_z\cdot(\vec{n}_w\cdot\bar{\bar{\tau}})\,dS} = -$$

$$\frac{2f\langle\bar{\rho}\rangle\langle\bar{u}\rangle\langle\bar{u}\rangle}{D}, \qquad (8)$$

with f being the friction factor and D the diameter. Similarly, relationships involving wall-fluid heat transfer coefficients are used to model the last term in (7) in single-phase flow, i.e., the wall heat flux.

In 2-phase flow, however, the empirical basis for such closure relationships is not well established, and an entirely new set for the interfield transfer of mass, momentum, and energy is needed. Therefore, while the 2-phase flow problem is not qualitatively different from the single-phase flow problem, it requires much more information in the form of closure relationships.

A problem also arises with terms on the left-hand side of (5), (6), and (7). In order to have the same number of variables as equations, we need to relate quantities like $\overline{\alpha_k\langle\rho_k u_k^2\rangle}$ to $\overline{\alpha_k}$, $\overline{\langle\rho_k\rangle}$, $\overline{\langle u_k\rangle^2}$. The problem also occurs in single-phase gas dynamics, where $\overline{\langle\rho_k u_k^2\rangle}$ must be related to $\overline{\langle\rho_k\rangle}$, $\overline{\langle u_k\rangle^2}$. To resolve this problem, the assumption is often made that the density and velocity profile is flat across the duct in single-phase flow. While this is reasonably accurate for turbulent flows, it may give substantially wrong answers in some cases, even in single-phase flow – see Bird *et al.* (1960). In 2-phase flow, density variations in the averaging volume are usually negligible; however, substantial variations in phase volume fraction ($\overline{\alpha_k}$) and velocity ($\overline{\langle u_k\rangle}$) may exist. Therefore, distribution effects are important in a wider range of problems.

Jump Conditions

Moving on to what is known about the closure relationships from the formal averaging procedure, all we have are the consistency relationships for interfield transfer. For 2 fields these jump conditions [see Banerjee and Chan (1980)] are

$$\sum_{k=1}^{2}\frac{1}{V}\int_{a_i}\bar{\dot{m}}_k\,dV = 0; \qquad (9)$$

$$\sum_{k=1}^{2}\frac{1}{V}\int_{a_i}\overline{[\dot{m}_k u_k + \vec{n}_z\cdot(n_k p_k) - \vec{n}_z\cdot(\vec{n}_k\cdot\bar{\bar{\tau}}_k)]}\,dS = 0; \text{ and} \qquad (10)$$

$$\sum_{k=1}^{2}\frac{1}{V}\int_{a_i}\overline{\left[\dot{m}_k\left(h_k + \frac{V_k^2}{2}\right) + p_k(\vec{n}_k\cdot\vec{V}_k) + \vec{n}_k\cdot(\vec{q}_k - \bar{\bar{\tau}}_k\cdot\vec{V}_k)\right]}\,dS. \qquad (11)$$

All other information regarding closure relationships has to be obtained from experiments, or from modelling and analysis external to the multifield model. In addition, we have the condition for phase volume fraction that

$$\sum_k \alpha_k = 1. \qquad (12)$$

The Equal Pressure Model

For the rest of the section, we will drop the overbar signs with the understanding that all quantities are ensemble averaged. The simplest multifield model is then obtained by putting the average pressures in each phase equal to each other within the averaging volume, and equal to the interfacial pressure, i.e., $\langle p_k\rangle = \langle p_{ki}\rangle =$

$\langle p \rangle$. In that case, the integral involving pressure on the right-hand side of the momentum equation (6) may be simplified by Gauss' theorem as

$$\frac{1}{V}\int_{a_i} \langle p\rangle \vec{n}_k \cdot \vec{n}_z \, dS = \langle p \rangle \frac{\partial \alpha_k}{dz}, \tag{13}$$

and (6) becomes

$$\frac{\partial \alpha_k \langle \rho_k u_k \rangle}{\partial t} + \frac{\partial \alpha_k \langle \rho_k u_k^2 \rangle}{\partial z} + \alpha_k \frac{\partial \langle p \rangle}{\partial z} - \alpha_k \langle \rho_k F_{kz} \rangle = -$$

$$\frac{1}{V}\int_{a_i} [\dot{m}_k u_k - \vec{n}_z \cdot (\vec{n}_k \cdot \bar{\bar{\tau}}_k)] \, dS + \frac{1}{V}\int_{a_{kw}} \vec{n}_z \cdot (\vec{n}_{kw} \cdot \bar{\bar{\tau}}_k) \, dS. \tag{14}$$

Since the pressure differences between phases are expected to be small over a cross-section, the equal pressure assumption is plausible at first sight. However, more careful consideration indicates gradients of the difference between phase pressures and interface pressures may be comparable to the other terms in the momentum equation. As shown in the next section, the terms involving pressure in the multifield momentum equations have a crucial effect on stability.

Structure and Validity of the Model

Separated Flows

Stratified Flow

Consider an incompressible stratified flow in the flow situation shown in Figure 2. If viscous effects are modelled by algebraic terms involving friction factors, as is conventional in single-phase flow, and we assume no heat or mass transfer, then the characteristics for the equal pressure, quasi-linear set of conservation equations (5) and (14) are wholly real only if

$$-\alpha(1-\alpha)\rho_1\rho_2(u_1 - u_2)^2 \geq 0, \tag{15}$$

where we have assumed $\langle u_k^2 \rangle = \langle u_k \rangle^2 = u_k^2$ (say). This is clearly impossible for 2-phase flow, so the characteristics are always complex and high-frequency instabilities may be expected [as discussed by Drew (1983), Ramshaw and Trapp (1978), and Banerjee and Chan (1980)]. The equal pressure model therefore cannot predict phenomena in stratified flows.

In the actual physical situation, the pressures are not equal. The form of the momentum equation can then be derived by writing

$$p_{ki} = \langle p_k \rangle + \Delta p_{ki} + \Delta p'_{ki}, \tag{16}$$

where

$$\Delta p_{ki} = \langle p_{ki} \rangle - \langle p_k \rangle$$

and

$$\Delta p'_{ki} = p_{ki} - \langle p_{ki} \rangle.$$

Since $\langle p_k \rangle$ and $\langle p_{ki} \rangle$ are constant in the averaging volume, therefore the term

$$\frac{1}{V}\int_{a_i} p_k \vec{n}_k \cdot \vec{n}_z \, dS = [\langle p_k \rangle + \Delta p_{ki}] \frac{\partial \alpha_k}{\partial z} + \frac{1}{V}\int_{a_i} \Delta p'_{ki} \vec{n}_k \cdot \vec{n}_z \, dS. \tag{17}$$

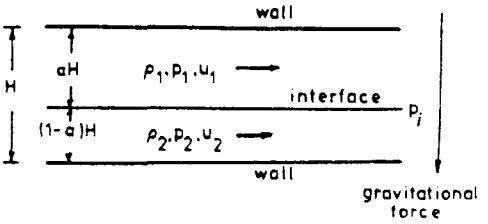

Figure 2 Schematic of stratified flow defining the symbols.

The linear momentum equation then becomes

$$\frac{\partial \alpha_k \langle \rho_k u_k \rangle}{\partial t} + \frac{\partial \alpha_k}{\partial z}\langle \rho_k u_k^2 \rangle + \alpha_k \frac{\partial \langle p_k \rangle}{\partial z} - \Delta p_{ki} \frac{\partial \alpha_k}{\partial z} =$$

$$-\frac{1}{V}\int_{a_i} [\dot{m}_k u_k + \vec{n}_z \cdot \vec{n}_k \Delta p'_{ki} - \vec{n}_k \cdot (\vec{n}_z \cdot \bar{\bar{\tau}}_k)] \, dS$$

$$+\frac{1}{V}\int_{a_i} \vec{n}_z \cdot (\vec{n}_{kw} \cdot \bar{\bar{\tau}}_k) \, dS. \tag{18}$$

To proceed, we now require expressions for Δp_{ki} and $\Delta p'_{ki}$ for the stratified flow situation in Figure 2; the pressure difference between phases may be expressed in the static approximation as

$$p_i - p_1 = \Delta p_{1i} = \rho_1 g \alpha H/2; \tag{19}$$

$$p_i - p_2 = \Delta p_{2i} = -\rho_2 g(1-\alpha)H/2. \tag{20}$$

At the level of this approximation, $\Delta p'_{ki}$ vanishes. Therefore, the right-hand side of the momentum equation is the same as (14), but the left-hand side now contains additional terms that are derivatives of α. Versions of this formulation were proposed by Rousseau and Ferch (1979), and Ardron (1980).

The condition for real characteristics is then

$$(\rho_2 - \rho_1) g H \left[\frac{\alpha}{\rho_1} + \frac{1-\alpha}{\rho_2}\right] \geq (u_1 - u_2)^2. \tag{21}$$

This is exactly the Kelvin-Helmholtz stability criterion for long waves. If the inequality is not satisfied, then interfacial instabilities will grow because the restoring forces due to gravity will not be sufficient to balance the sucking action at the wave crest due to Bernoulli's effect. The criterion in (21) signals a transition to slug flow. (In reality, transition may occur earlier due to non-linear effects; see Ahmed and Banerjee (1985).) Consideration of phase pressure differences, then, captures a real physical effect.

The static approximation in (19) and (20) breaks down for finite amplitude waves. Banerjee (1980) has integrated the transverse momentum equation and shown that higher order terms occur that lead to a Korteweg-DeVries equation for interfacial waves at the next level of approximation.

Inverted Annular Flow

We will consider another example of a separated flow to illustrate the capability of the model to predict rather complex phenomena.

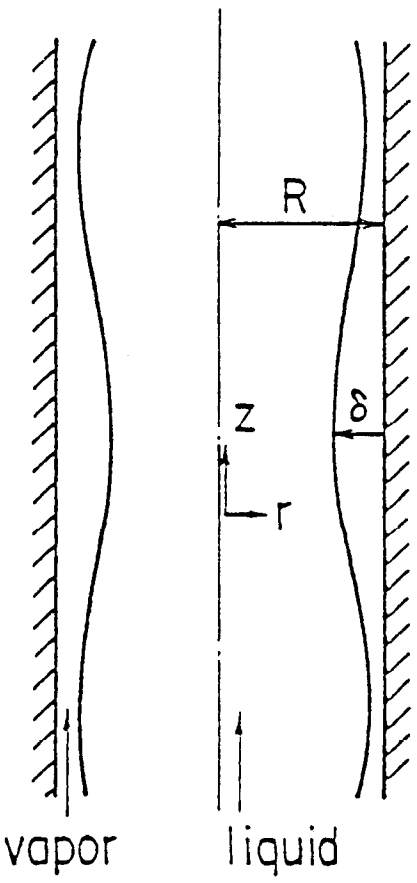

Figure 3 Schematic of inverted annular flow.

Inverted annular flows similar to the schematic in Figure 3 often occur during reflood and rewetting of vertical tubes. The wall may be thought of as being very hot, and a film of vapor is generated that prevents the liquid from wetting the wall. The vapor-liquid interface is wavy, and this enhances heat transfer compared to condensation through a uniform laminar vapor film. To model such a situation, the pressure difference between the phases due to surface tension must be incorporated into the momentum equations. The momentum equation for the liquid then becomes (dropping the averaging signs)

$$\rho_2\alpha_2\frac{\partial u_2}{\partial t}+\rho_2 u_2\alpha_2\frac{\partial u_2}{\partial z}+\alpha_2\frac{\partial p_1}{\partial z}-\frac{\sigma}{2R\sqrt{\alpha_2}}\frac{\partial\alpha_2}{\partial z}-\frac{\sigma R\sqrt{\alpha_2}}{2}\frac{\partial^3\alpha_2}{dz^3}=$$

algebraic terms that do not affect phase speed. (22)

Note that the reference pressure is p_1, i.e., the pressure in the vapor; σ is the surface tension; R is the tube radius; and we have assumed distribution coefficients ~1.0.

If a linear stability analysis is performed for the conservation equations, assuming the phases are incompressible, we find the phase speed is real if

$$(u_1-u_2)\le\left[\frac{k^2\sigma R}{2\sqrt{\alpha_2}}-\frac{\sigma}{2R\alpha_2^{3/2}}\left(\frac{\alpha_1}{\rho_1}+\frac{\alpha_2}{\rho_2}\right)\right]^{1/2}, \tag{23}$$

where k is wave number.

Interfacial mass transfer has only a weak effect on this criterion. In particular, the short wavelengths (large k) are stable even at very high velocity differences between phases.

The length of the most unstable waves can be found by seeking the maximum growth factor. Kawaji and Banerjee (1986) show that this wavelength is given by

$$\alpha=\frac{2\pi_2^{1/4}(\sigma R)^{1/2}}{\dfrac{\alpha_2\rho_2\rho_1(u_1-u_2)^2}{\alpha_1\rho_2+\alpha_2\rho_1}+\left[\dfrac{\sigma}{2R\sqrt{\alpha_2}}\right]^{1/2}}. \tag{24}$$

As shown in Figure 4, this result compares extremely well with the experimental data of De Jarlais (1983).

Dispersed Bubbly Flows

While the multifield model may be expected to predict separated flows with accuracy, its application to more closely coupled flows is less obvious. This is because great care has to be taken in considering forces arising out of the pressure variation over interfaces, i.e., the term involving $\Delta p'_{ki}$ on the right-hand side of (18) requires attention.

To illustrate the problem, consider forces on an assemblage of spheres spaced sufficiently far apart that interactions are weak. The situation is shown schematically in Figure 5. Let the continuous phase be incompressible, inviscid, and without circulation. Pauchon and Banerjee (1985) have shown for this case that the governing equations are of the form:

$$\frac{\partial\alpha_1}{\partial t}+u_1\frac{\partial\alpha_1}{\partial z}+\alpha_1\frac{\partial u_1}{\partial z}=0, \tag{25a}$$

$$\frac{\partial\alpha_1}{\partial t}+u_1\frac{\partial\alpha_1}{\partial z}+\alpha_1\frac{\partial u_1}{\partial z}=0, \tag{25b}$$

$$\rho_1\alpha_1\frac{D_1u_1}{Dt}+\alpha_1\frac{\partial p_1}{\partial z}=-\frac{1}{2}\rho_2\alpha_1\left(\frac{D_1u_1}{Dt}-\frac{D_2u_2}{Dt}\right), \text{ and} \tag{25c}$$

$$\rho_2\alpha_2\frac{D_2u_2}{Dt}+\alpha_2\frac{\partial p_2}{\partial z}=\Delta p_{2i}\frac{\partial\alpha_2}{\partial z}+\frac{1}{2}\rho_2\alpha_1\left(\frac{D_1u_1}{Dt}-\frac{D_2u_2}{Dt}\right), \tag{25d}$$

where

$$\Delta p_{2i}=-\frac{1}{4}\rho_2(u_1-u_2)^2 \tag{25e}$$

and $\Delta p_{1i}=0$.

The material derivative $D_k/Dt=\partial/\partial t+u_k\partial/\partial z$. The last term on the right-hand side of (25c) and (25d) arises from the accelerations of the continuous and dispersed phases and is sometimes called the 'virtual mass' term. The first term on the right-hand side of (25d) arises from the difference between the average continuous phase pressure and the average interfacial pressure. This difference is straightforward to calculate for spheres and is given in (25e). Clearly, the $\Delta p_{2i}\,\partial\alpha_2/\partial z$ term vanishes if the phase volume fraction gradients vanish; therefore it does not appear for a single sphere in a large averaging volume.

There is still considerable controversy over the form

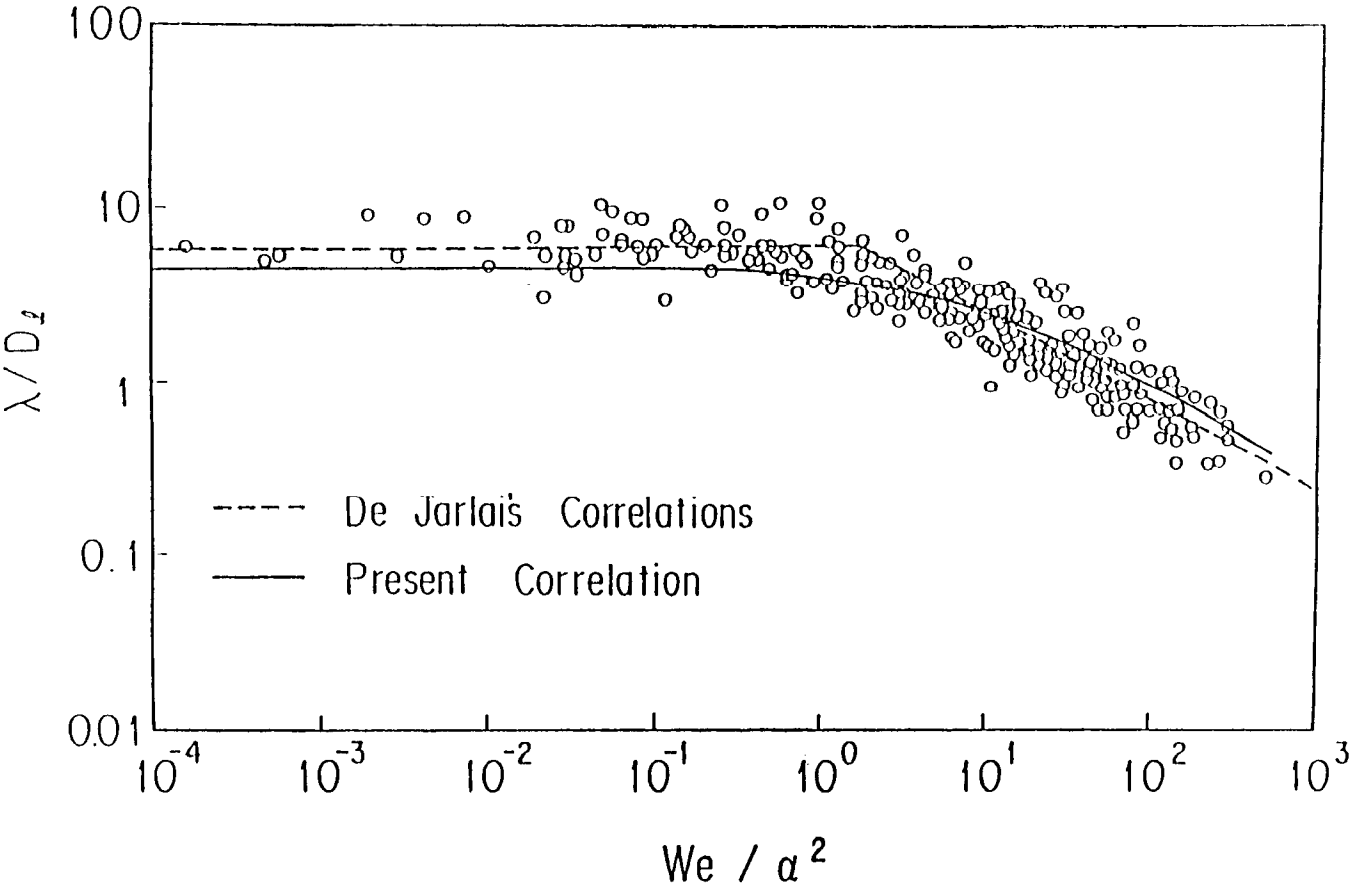

Figure 4 Comparison of predictions with De Jarlais' data.

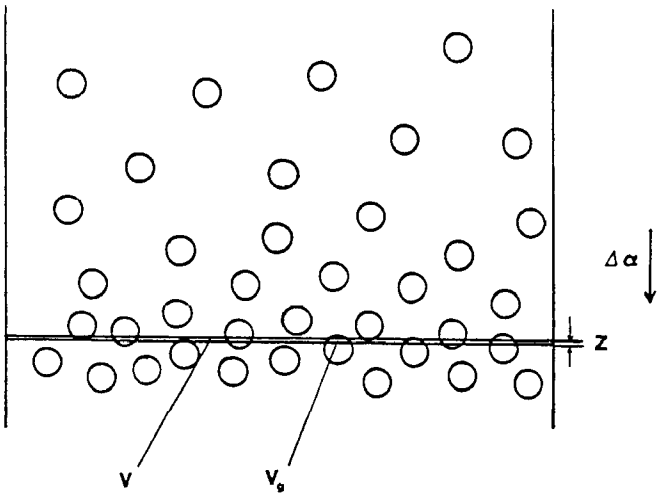

Figure 5 Schematic of bubbly flow showing averaging volume.

of (25c) and (25d). Drew *et al.* (1979) suggest that the acceleration should be 'objective' and the virtual mass term should then contain an additional derivative of the form $(u_1 - u_2)\,\partial/\partial z\,(u_1 - u_2)$. We are not as yet certain whether (25c) and (25d) are correct or Drew *et al.*'s form is correct. In any case, we will proceed to study the stability of the system (25a)–(25e).

Pauchon and Banerjee (1985) have shown that the characteristics for (25) with $\rho_1 \ll \rho_2$ are

$$\lambda^* = \frac{\alpha_2}{2 + 4\alpha_1\alpha_2} + \sqrt{\Delta}/(1 + 2\alpha_1\alpha_2), \tag{26}$$

where

$$\lambda^* = \frac{\lambda - u_2}{u_1 - u_2}$$

and

$$\Delta = \frac{\alpha_2^2}{4} - \alpha_1\alpha_2\left(\frac{1}{2} + \alpha_1\alpha_2\right).$$

These characteristics give the void propagation velocity and are wholly real for

$$\alpha_1 \lesssim 0.26. \tag{27}$$

The model, therefore, predicts a transition to a qualitatively different flow regime when $\alpha_1 > 0.26$. This is approximate because the coefficient for the virtual mass term and Δp_{2i} is based on an assembly of non-interacting spheres of constant radius. As the phase volume fraction increases, interactions increase, and some modification to the criterion may be expected, i.e., the

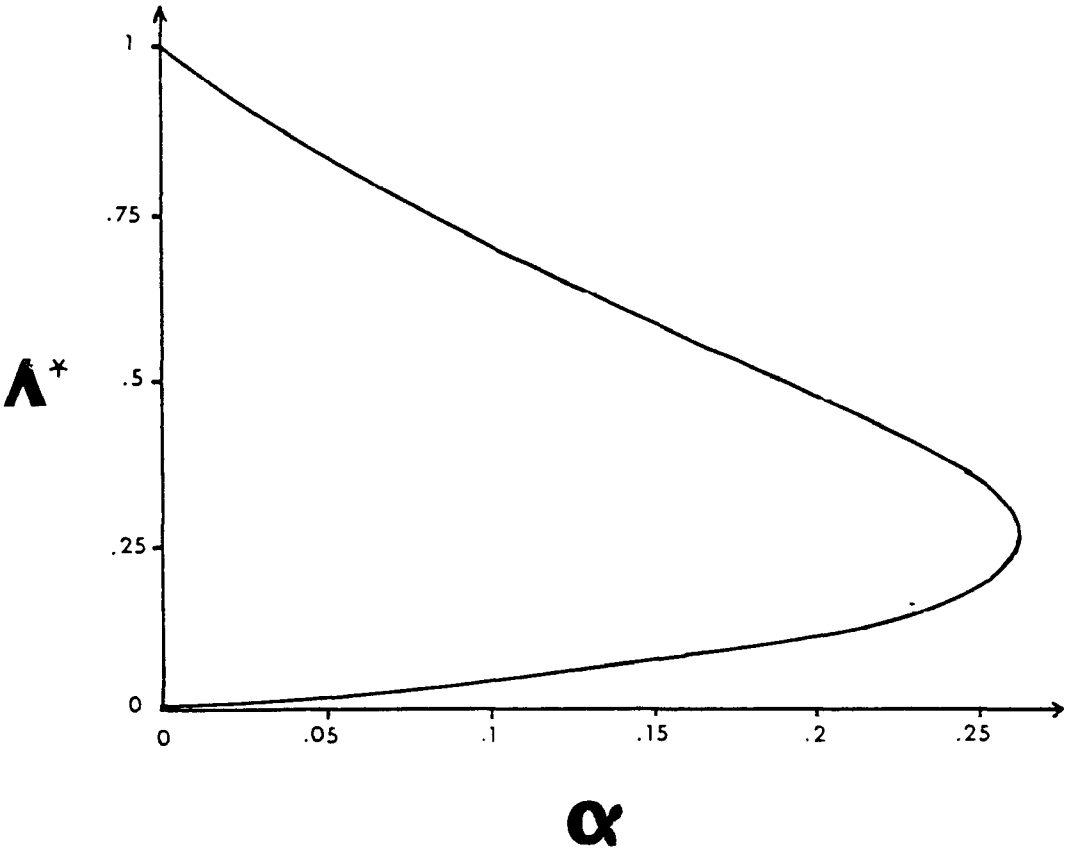

Figure 6 Plot of the non-dimensional characteristic velocity against void fraction.

transition is probably slightly wrong. The solution for λ^* given in (26) is plotted in Figure 6. The void propagation velocities lie between velocities for the continuous and dispersed phase. Therefore, measurement of void propagation (say, by cross-correlation techniques) does not give the velocity of either phase. To determine whether the model is correct, comparisons have been made with the data of Bernier (1981) and Pauchon and Banerjee (1985). Plots of the predictions and experimental data are shown in Figures 7 and 8. It is evident that the agreement is quite excellent even at relatively high gas velocities. This is an indication that the main features of the model are correct even when the phases are closely coupled.

Dispersed Droplet Flow

A similar analysis, as for dispersed bubbly flow, can be performed for droplet flow, but a fifth equation is needed to complete the system of equations, since an additional dependent variable R_d has to be introduced to the system through the pressure difference term. In terms of this added variable, the liquid volume fraction can be expressed as follows:

$$\alpha_l = \frac{4}{3}\pi R_d^3 n,$$

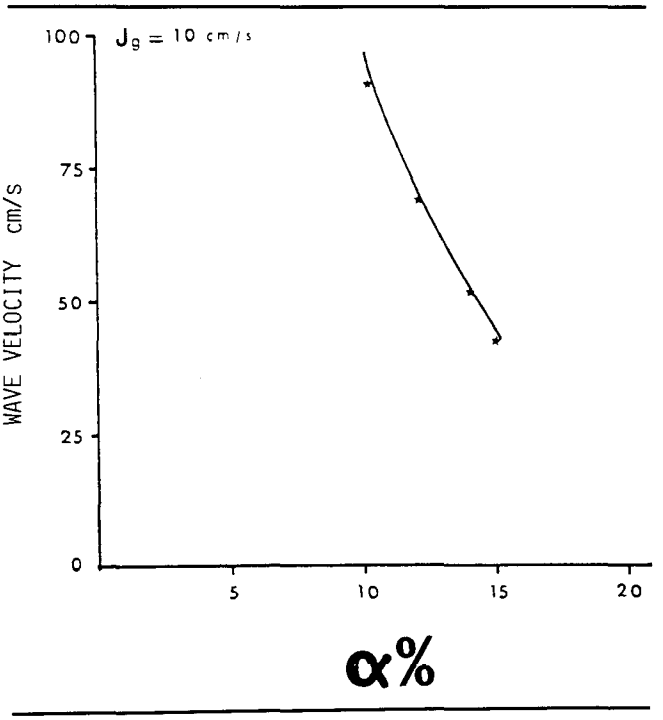

Figure 7 Void propagation velocity-predictions compared with data of Pauchon and Banerjee (1985). The liquid superficial velocity is $0.0884 \leq j_2 \leq 0.765$ m / s.

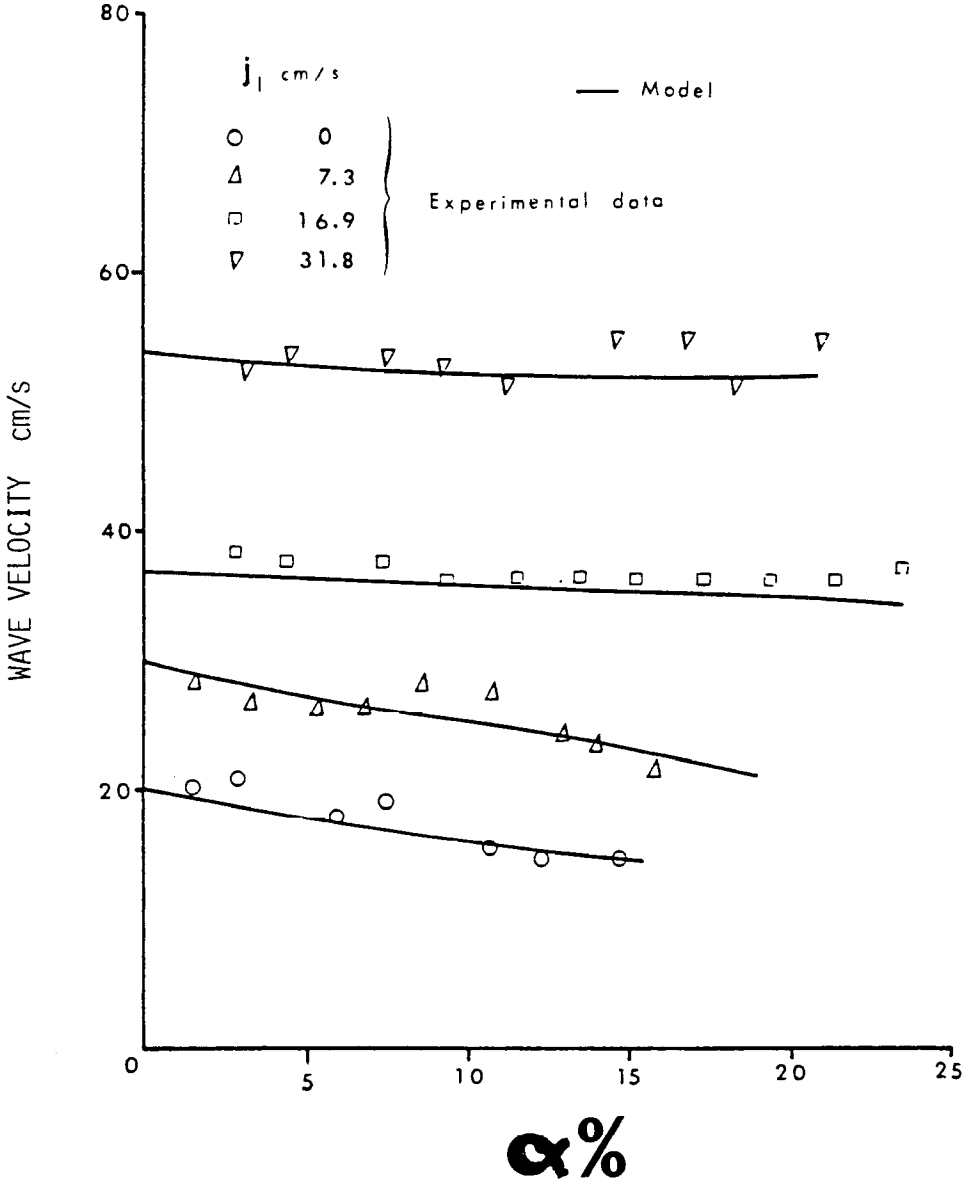

Figure 8 Predictions of void propagation velocity compared with Bernier (1981) data with $0 \leq j_2 \leq 0.318$ m / s.

where n = number density of drops. As the drops travel along the flow channel, both n and R_d change, resulting in net variation of α_l. Note that we subscript with l for liquid, v for vapor, and d for droplet in this section to distinguish the results from the previous one.

In the present analysis, the variables n and R_d are used instead of α_l as the fourth and fifth dependent variables, in addition to U_l, U_c, and P_v. To complete the hydraulic equation system, however, a fifth equation is necessary. For this, we consider a simple problem of the behaviour of a droplet of radius R_d subjected to a gas stream with a relative velocity U_r. For such a droplet, the external pressures at the forward and rear stagnation points ($\tau = 0$ and π, respectively) and at the equator ($\theta = \pi/2$) are given, respectively, by the following equations

$$P_{vi}(\theta = 0 \text{ or } \pi) = P_v + \frac{1}{2}\rho_v U_r^2; \tag{28}$$

$$P_{vi}(\theta = \pi/2) = P_v - \frac{5}{8}\rho_v U_r^2. \tag{29}$$

Due to this external pressure difference, the droplet is expected to be pressed at stagnation points, deforming into an oblate spheroidal shape, which is an ellipsoid formed by rotating an ellipse about its minor axis. Unless the droplet breaks up, these forces tending to deform the droplet are balanced by surface tension, which tends to restore a spherical shape. Photographic observations of liquid drops, either suddenly intro-

duced into an air stream [Haas (1976)] or moving at a steady speed [Ryan (1976)] show clearly that the drops become flattened and spheroidal in shape. Ryan's experiments involving drops of water with surfactant added to reduce surface tension further show that the degree of flattening increases with decreasing surface tension, as expected.

For the present analysis, we assume that the semi-minor and semi-major axes of the spheroid at equilibrium state are equal to a and b, respectively. Furthermore, we assume the potential flow about a sphere is still applicable and can approximate the pressure distribution on the surface of a spheroid. Then, at equilibrium, the following relationship must hold between the dynamic pressure and surface tension at the stagnation points and at the equator, respectively:

$$P_l - P_v - \frac{1}{2}\rho_v U_r^2 = \frac{2\sigma}{R_d} X^2 \tag{30}$$

and

$$P_l - P_v + \frac{5}{8}\rho_v U_r^2 = \frac{\sigma}{R_d}(X^{1/2} + X^{-5/2}), \tag{31}$$

where $X = a/R_d$ (shape factor). Subtracting equation (30) from (31), and rearranging, we obtain the following equation describing the degree of flattening the droplet is subjected to in order to balance the forces originating from the dynamic pressure of the vapor phases:

$$We = \frac{\rho_v U_r 2R_d}{\sigma} = \frac{16}{9}(X^{1/2} + X^{-5/2} - 2X^2). \tag{32}$$

A non-dimensional parameter appearing on the left-hand side of equation (32) is identified to be the Weber number defined in terms of the droplet's mean diameter and relative velocity. As the relative velocity, or Weber number, is increased, the droplet is predicted to become more flattened in shape, as expected from physical intuition. The use of pressure distribution for the potential flow about a sphere rather than a spheroid tends to overestimate the degree of flattening for a given Weber number; however, we adopt the present approach to simplify the analysis. If a more accurate description is desired, an analytical solution for potential flow about an oblate spheroid should be used instead.

To obtain the fifth equation necessary for the stability analysis, we assume that the shape factor remains constant and differentiate equation (32) with respect to z (or t). The following equation is obtained to complete the equation system for stability analysis:

$$\frac{2}{U_r}\frac{dU_r}{dz} + \frac{1}{R_d}\frac{dR_d}{dz} = 0. \tag{33}$$

Performing a similar analysis as described for the inverted annular flow, the following dispersion relation for the droplet flow is obtained

Table 1: Critical Weber Number for Various Density Ratios and Void Fractions

	α_v					
l_l/l_v	*0.3*	*0.5*	*0.7*	*0.9*	*0.95*	*1.0*
10	20.95	10.75	8.96	8.23	8.11	8.0
100	19.22	10.68	8.96	8.23	8.11	8.0
1000	19.22	10.67	8.96	8.23	8.11	8.0

$$\left(\frac{\omega}{k}\right) = \frac{\rho_l U_l + {}_c\rho_v U - 4\sigma/R_d U_r}{\rho_l + \rho_v} = \left[\frac{64\sigma^2}{R_d^2 U_r^2} + \frac{16\sigma}{R_d}(\rho_l - \rho_v) + \rho_v U_r^2\left(\frac{\alpha_l}{\alpha_v}(\rho_l + \rho_v) - 4\rho_l\right)\right]^{1/2}/2(\rho_l + \rho_v). \tag{34}$$

For stability, the condition given below has to be satisfied:

$$We < \frac{16(\beta - 1) \pm 16[(\beta + 1 - \alpha_l/\alpha_v)(\beta + 1)]}{\beta(5 - 1/\alpha_v) - 1/\alpha_v + 1}, \tag{35}$$

where

$$\beta = \rho_l/\rho_v. \tag{36}$$

We first note that in the limit $\alpha_v = 1.0$, equation (34) simplifies to

$$We < 8. \tag{37}$$

The stability criterion obtained above implies breakup of drops for a given dispersed flow system when the Weber number, defined by equation (32), exceeds a critical value.

For various density ratios and void fractions, the values of the critical Weber number predicted by equation (34) are tabulated in Table 1. The effect of density ratio is small. As void fraction is decreased from unity, the critical Weber number is predicted to increase gradually. The validity of this predicted behaviour is not clear at present due to the lack of experimental data concerning the breakup of drops in a confined flow channel.

An infinitely large critical Weber number is obtained as void fraction decreases to a value of 0.2. In reality, however, dispersed flow usually exists for void fractions greater than about 0.8. At lower values, droplet coalescence, collision, and breakup processes will be important, and the present analysis no longer applicable. It is also noted here that the present analysis is limited to the well-established dispersed flow, for example, in regions well downstream of the inverted annular flow in reflooding of a hot vertical tube. The assumption of potential flow about a sphere has limited validity in the transition region, where the liquid core in inverted annular flow destabilizes and breaks up into slugs, ligaments, and various large and small droplets. In this region, the mechanisms responsible for droplet breakup may be quite different from those relevant to well-developed dispersed flow with high

void fraction, and the situations of droplet breakup in a free gas stream are discussed below.

The breakup of drops of a free gas stream has been investigated in the past, both experimentally and theoretically. For cases where the inertial force and surface tension dominate the viscous effects, the droplet breakup can be specified by a critical Weber number [Hinze (1955)]. Hinze (1948) suggested further that the value of the critical Weber number should depend on the rate of droplet acceleration with respect to the gas stream. Various cases have been investigated in the past, ranging from a drop suddenly exposed to a high-velocity gas stream to that of a drop moving in a gas stream at a terminal speed. For these two extreme cases, Hinze (1955) recommends critical Weber numbers of 13 and 22, respectively.

The experimental data of Haas (1976) for the breakup of mercury drops in air indicate a critical value of 10, while Hanson *et al.* (1963) obtained values ranging from 7 to 17 for the breakup of water and methyl alcohol drops by air blast. On the other hand, the experimental data of Lane (1951) and Ryan (1976), involving a water drop placed in a vertical wind tunnel and held stationary by an upward flow of air, indicate critical values of 10 and 12, respectively. Wallis (1974) suggests that a drop moving in an infinite medium at its terminal speed will break up at a critical Weber number equal to 8, in agreement with equation (37). Kataoka *et al.* (1983) also suggests a critical Weber number of 8–17 for a large drop falling at its terminal speed.

The stability criterion derived from the present analysis is consistent with the available data on droplet breakup in a gas stream. Furthermore, Ryan's data (1976) indicate that the degree of maximum flattening before breakup, defined by the ratio a/b, is nearly constant at a value of 0.4 for drops of varying surface tension, and maximum equivalent spherical diameter between 4.4 mm and 9.1 mm. The limiting value of a/b equal to 0.4 corresponds to the shape factor a/R_d of 0.54 and, from equation (32), the Weber number of 8.4, which is also close to the critical value found in the present stability analysis.

If the ΔP_{vi} term is neglected in the above analysis, then the stability condition expressed by equation (37) is obtained for all void fractions and density ratios. This shows that the ΔP_{vi} term accounting for the nonuniformity of the interfacial pressure distribution tends to enhance the stability of the dispersed flow system, a result consistent with that reported by Pauchon and Banerjee (1986).

Rewetting of Horizontal Channels

The preceding methodology can be applied to the study of rewetting and refilling of a horizontal tube. The details are given in Chan and Banerjee (1981a, b, c).

Consider the flow situation shown in Figure 9. We

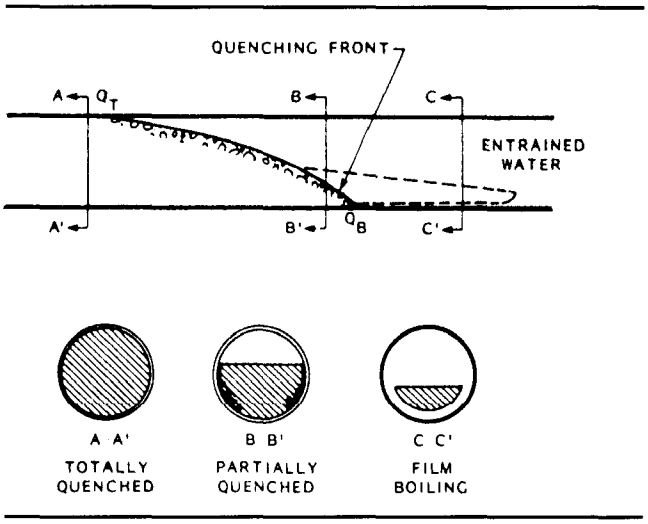

Figure 9 Characteristics of horizontal channel rewetting.

can write sets of conservation equations for the liquid and the vapor, i.e., a 2-field model. This ignores bubbles in the liquid and droplets in the vapor, but appears to be a reasonable assumption for subcooled conditions at the quench front.

The mass and momentum conservation equations may then be phrased as

$$\frac{\partial \bar{U}}{\partial t} + \bar{A}\frac{\partial \bar{U}}{\partial z} = \bar{E}, \tag{38}$$

where

$$U = \begin{bmatrix} h_L \\ U_L \end{bmatrix}, \quad A = \begin{bmatrix} U_L & y_h \\ g & U_L \end{bmatrix}, \quad E = \begin{bmatrix} E_1 \\ E_2 \end{bmatrix},$$

and U_L is the liquid velocity, h_L is the height of liquid in the pipe, g is gravitational acceleration, $y_H = \alpha_L/(\partial\alpha_L/\partial\alpha_L)$, α_L is the fraction of the cross-sectional area occupied by the liquid, and E_1 and E_2 are terms involving wall and interfacial friction, vaporization rate, and gas phase inertia.

Some simplifications have gone into deriving these equations, and these are discussed in more detail in Chan and Banerjee (1981b). The bulk liquid temperature, T_L, is given by the energy balance

$$\frac{\partial(\alpha_L T_L)}{\partial t} + \frac{\partial}{\partial z}(\alpha_L U_L T_L) = \left(\frac{1}{\rho C}\right)\left[k_L \frac{\partial}{\partial z}\left(\alpha \frac{\partial T_L}{\partial z}\right) + (1-\beta)q^{111}\right], \tag{39}$$

where q^{111} is the heat flux per unit volume and depends on the mode of heat transfer; e.g., for refilling and rewetting problems, it may assume different values for the film boiling (or precursor cooling) region, and the wet (boiling or forced convection to liquid) region. Chan and Banerjee (1981c) discuss the applicable relationships in detail.

$(1-\beta)$ is the fraction of energy input that goes into

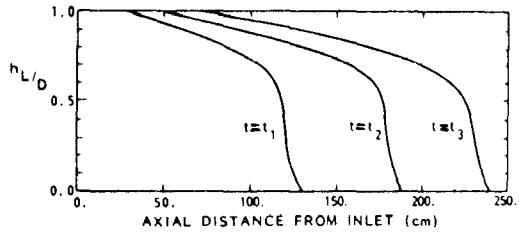

Figure 10 Propagation of refilling front.

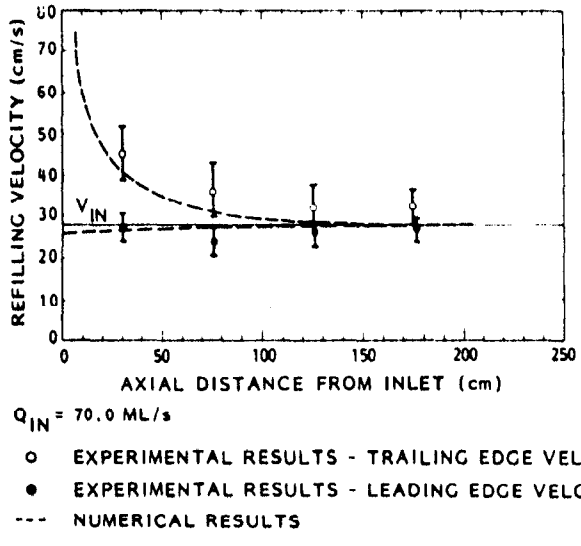

Figure 11 Refilling velocities – Q_{in} = 8–.0 ml / s.

heating the liquid phase. This is not known *a priori*, and it is necessary to make a model for energy partition to heat the liquid and cause vaporization.

The hydraulic equations (38) can be solved to determine whether the relatively simple problem of refilling a horizontal cold tube can be predicted. If the refilling process is started by suddenly opening a valve, then the refilling front propagates with the shape shown in Figure 10. Note that the leading edge propagates faster than the trailing edge. The velocity of the leading edge and trailing edge of the front are compared with experiments in Figure 11. It is clear that the theoretical predictions are in agreement with the experiments, which gives confidence in the 2-field model in (38).

If the tube is hot, so that the refilling front moves faster than the rewetting (or quench) front, as in Figure 10, then a rewetting criterion is necessary for predictions. As discussed previously, a criterion based on temperature is not satisfactory. This is because the rewetting temperature can be very different at different axial and circumferential locations. A model for rewetting has therefore been proposed by Banerjee and Chan (1981c).

The model postulates that film boiling is maintained

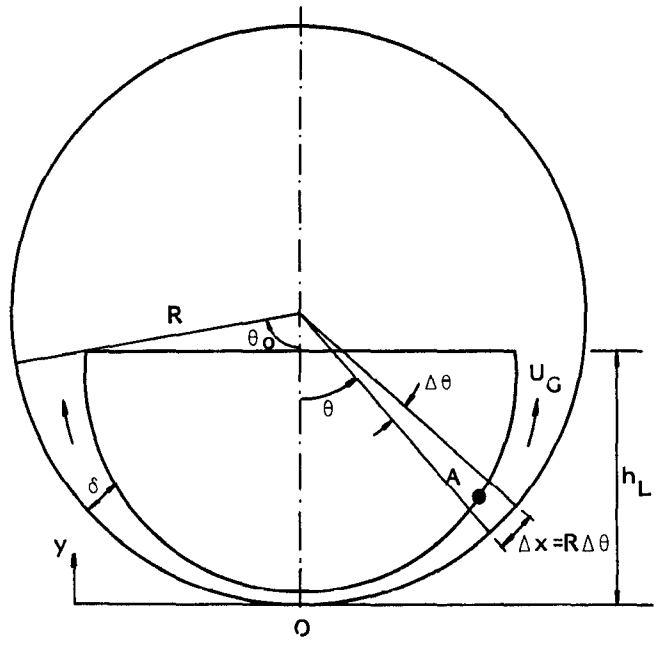

Figure 12 Film boiling model.

because the circumferential vapor flow, as shown in Figure 12, supports the liquid – much like a Hovercraft. However, as the depth of the liquid in the tube increases, the vapor velocity needed to support it also increases. At some depth, the vapor velocity may become sufficient to excite the Kelvin-Helmholtz instability, as discussed earlier. This in itself is only a necessary, but not sufficient, condition for rewetting. The sufficient condition is that the enhancement in local heat transfer due to the instability must be much larger than the conduction heat transfer from the surrounding region. Only then can the cooled regions grow rapidly, leading to rewetting. However, for a thin-walled pipe with low thermal capacitance, conduction in the wall is small. Therefore, for thin-walled pipes, onset of an interfacial instability may lead to rewetting; i.e., is both necessary and sufficient. The onset of the interfacial instability can be related to the depth of liquid through the circumferential velocity. Therefore, the rewetting criteria is phrased in terms of the depth of the liquid.

The model was tested against experimental data, and the results are shown in Figure 13. The two lines are for the first 2 modes of the instability. It is clear that the data fall between the predictions for the modes, and are largely independent of the initial wall temperature.

If this rewetting mechanism is introduced into the 2-field model, i.e., to give q^{111} in (39), then the wall temperatures can be predicted. The theoretical and experimental results are compared in Figure 10. The agreement is good, considering the complexity of the phenomena. In particular, note that the top (say, TET) rewets later than the bottom (TEB) at any location (say,

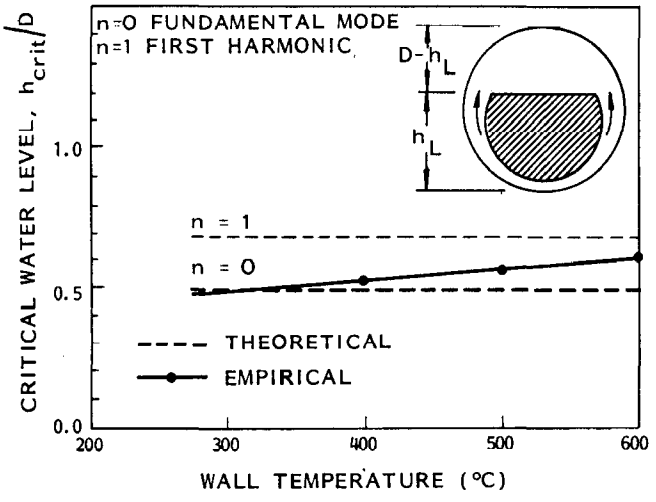

Figure 13 Comparison of theoretical and empirical water level for vapor film instability.

E). Also, the bottom shows much greater precursor cooling due to the liquid tongue and film boiling.

The theoretical rewetting velocities for different injection rates and wall temperatures are compared with

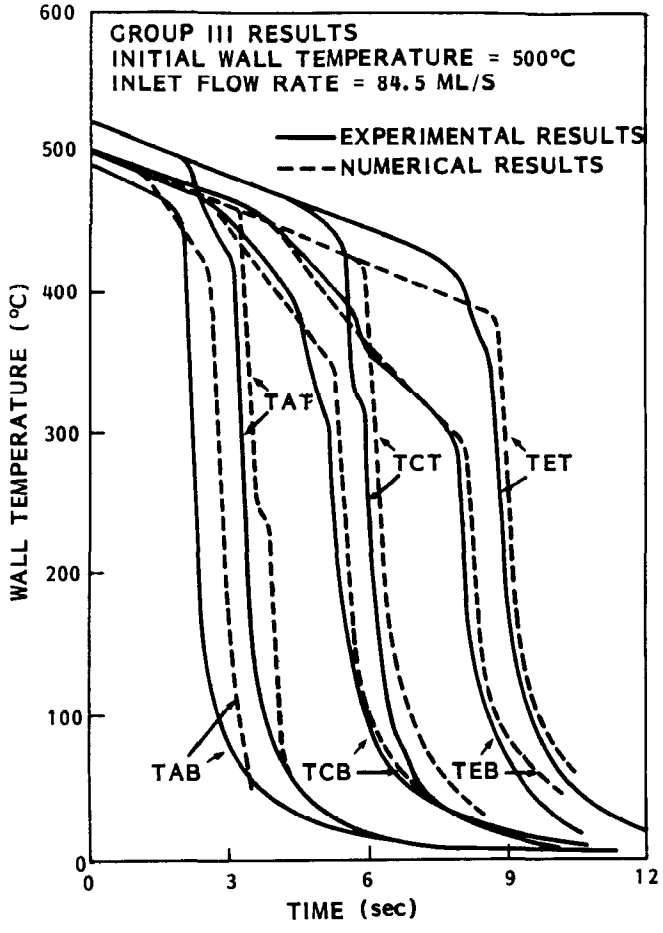

Figure 14 Transient top and bottom wall temperatures – comparison of experimental and numerical results.

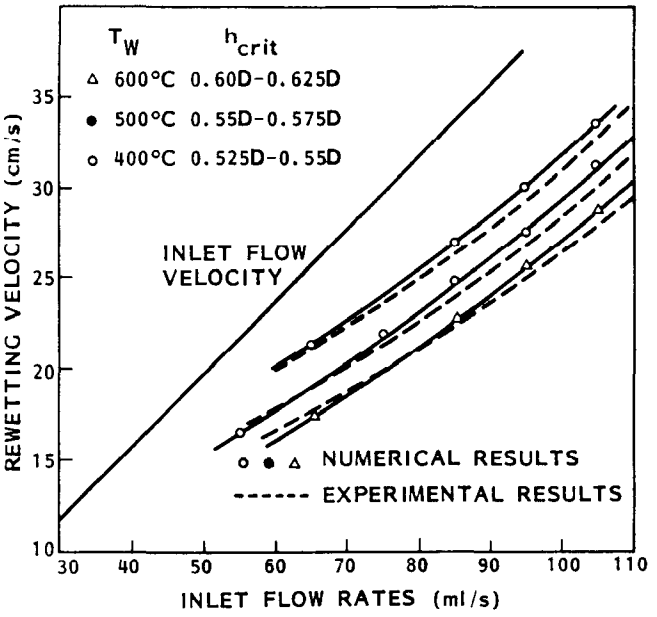

Figure 15 Average rewetting velocity versus inlet flow rate – comparison of experimental and numerical results.

data in Figure 15. Again, it is clear that the agreement is good. Note that the model does not use adjustable parameters to improve the 'fit' and is based on the simple postulate that rewetting coincides with the onset of an interfacial instability, when the wall is thin.

Limitations of the Model

The preceding discussion illustrates that the multifield model can predict a variety of phenomena without adjustment, or 'tuning,' of coefficients. It works well for both separated and closely coupled flows, provided the closure relationships or interactions between fields are developed with care, and attention is paid to the physics of the flow situation.

We turn now to the closure relationships required for forces at the wall and between fields due to viscous effects, i.e., the terms containing τ in (18), and the part of the $\Delta p'_{ki}$ time affected by viscosity – called form drag in Bird *et al.* (1960). For the multifield model these terms are written by analogy with single-phase flow, so the forces are expressed as:

$$\text{total drag (form + friction)} = -\frac{1}{8}\rho_c a_i C_D(\langle\overline{u_c}\rangle - \langle\overline{u_d}\rangle)\,|\langle\overline{u_c}\rangle - \langle\overline{u_d}\rangle|$$

for submerged objects;

$$\text{frictional drag} = -\frac{1}{2}\rho_c a_i f(\langle\overline{u_c}\rangle - \langle\overline{u_d}\rangle)\,|\langle\overline{u_c}\rangle - \langle\overline{u_d}\rangle|$$

for separated flows; and

$$\text{wall drag} = -\frac{1}{2}\rho_c a_{kw} f\langle\overline{u_c}\rangle\,|\langle\overline{u_c}\rangle|\,, \qquad (40)$$

where a_i and a_{kw} are the interfield and wall areas per unit volume, C_D is a drag coefficient, f is friction factor,

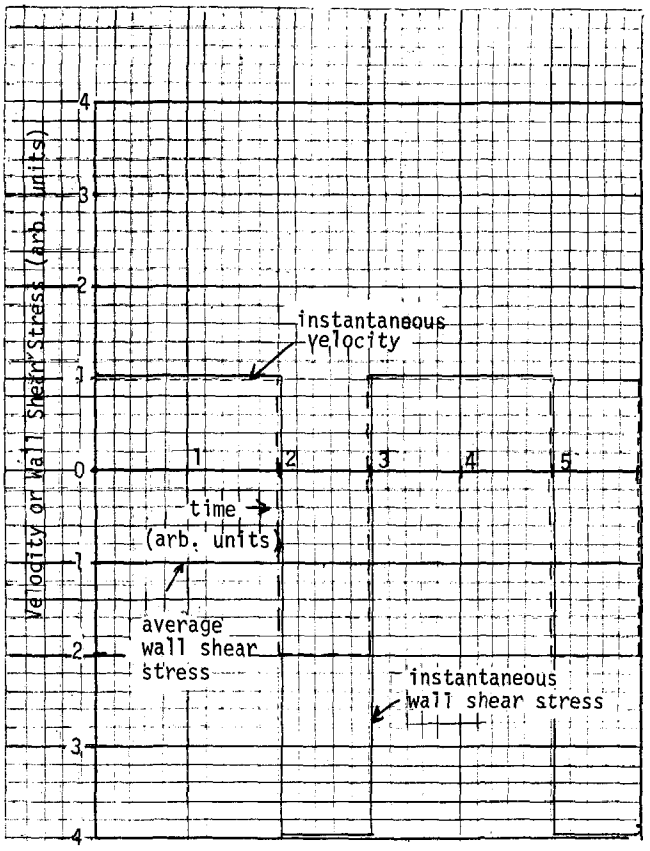

Figure 16 Schematic showing instantaneous velocity with mean velocity = 0, and instantaneous and average wall shear stress. The wall shear stress varies as the square of the velocity.

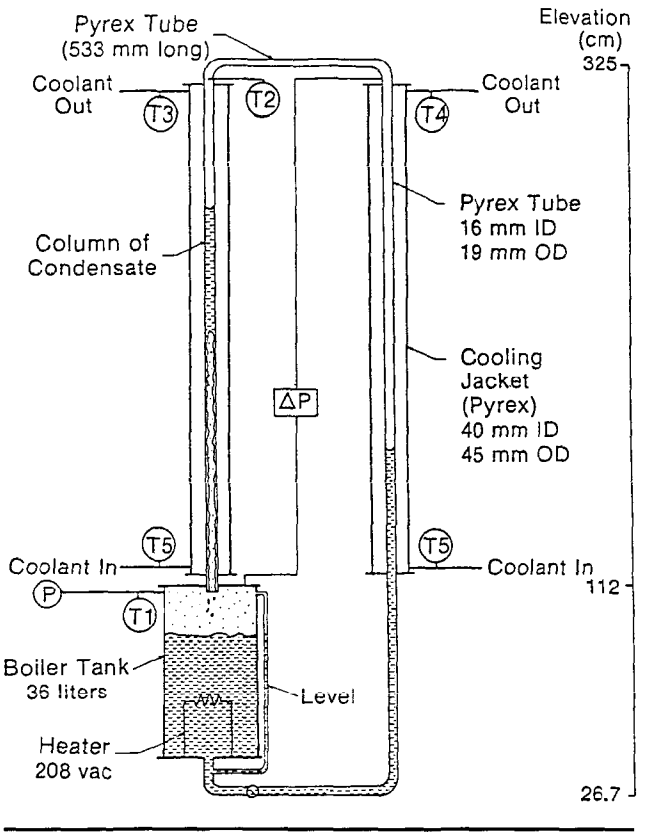

Figure 17 Schematic of experimental apparatus showing fluid distribution during refluxing near the flooding point.

and subscripts c and d denote continuous and dispersed phases, respectively. The absolute value signs are used to take flow reversal into account, so that the force points in the right direction.

For each flow regime, expressions have been developed for the unknowns in (40) [see, for example, Ransom *et al.* (1984); the TRAC-PD2 manual (1982); and Banerjee (1985)].

A difficulty arises, however, when flows are oscillatory. Consider a flow and wall shear stress history shown schematically in Figure 16. Here the time-averaged flow vanishes. However, the time-averaged wall shear stress does not because it is proportional to the sphere of the velocity. Thus expressions like (40) do not predict wall (or interfacial shear stress) in such situations.

To illustrate this, some data on flux condensation is presented. The physical situation for refluxing near the flooding point is shown in Figure 12. Vapor flow is introduced at the bottom of a vertical pipe, flows upwards, and condenses. The liquid, on the average, runs downward countercurrent to the vapor flow.

This situation is of importance in assessing small break accidents in pressurized water reactors. A scenario which has been observed in experiments is shown in Figure 18. Here, steam is formed in the reactor core and flows to the steam generators, where it condenses, and the condensate runs back countercurrent to the steam flow. However, if the steam flow is slightly above the flooding value, the steam generators do not drain completely on the riser side and liquid is held up, as shown in the figure. The liquid head exerts back pressure on the core and causes the liquid level to drop. In certain cases, portions of the core may be uncovered.

It is therefore important to predict the liquid inventory distribution in the system and, particularly, on the riser side of the steam generators. This is impossible to do on the basis of shear stress correlations of the form in (40).

To demonstrate this, data on liquid and vapor velocities and void fraction are plotted in Figure 19. The average liquid flow is downward and the average vapor flow is upward, as shown in the figure. A single-phase region exists above the condensing 2-phase region, i.e., above the point at which α goes to zero.

The average wall shear stress is plotted in Figure 20, together with the quantity $\langle u_2 \rangle |\langle u_2 \rangle|$. It is evident the average wall shear stress goes through a change in sign. The average wall shear stress, if modelled by an expression of the type in (40), would indicate that the flow at the bottom of the condenser is upward, and

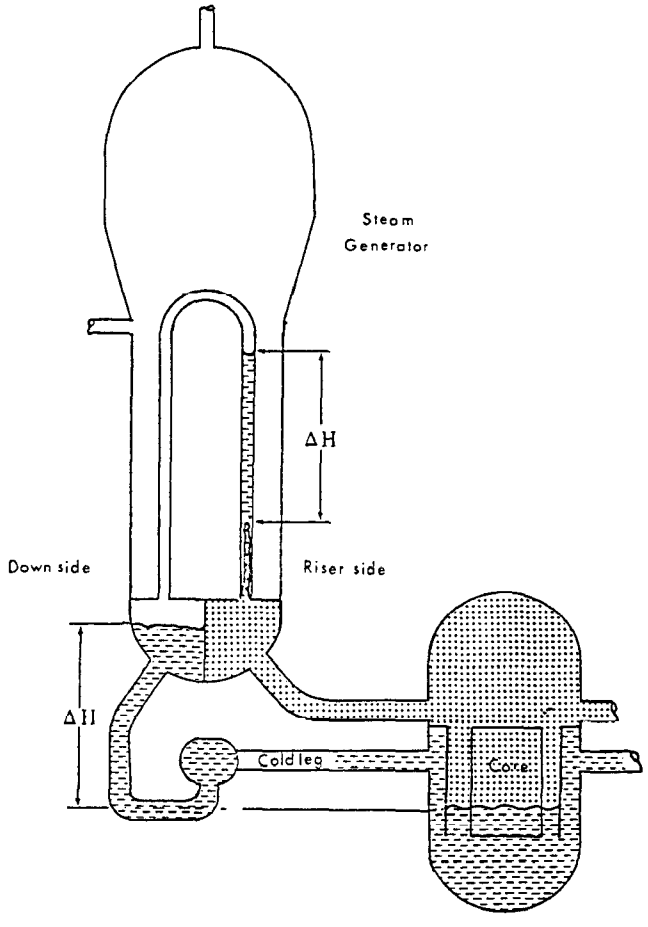

Figure 18 Small break accident scenario with steam generation rate leading to flooding during reflux condensation.

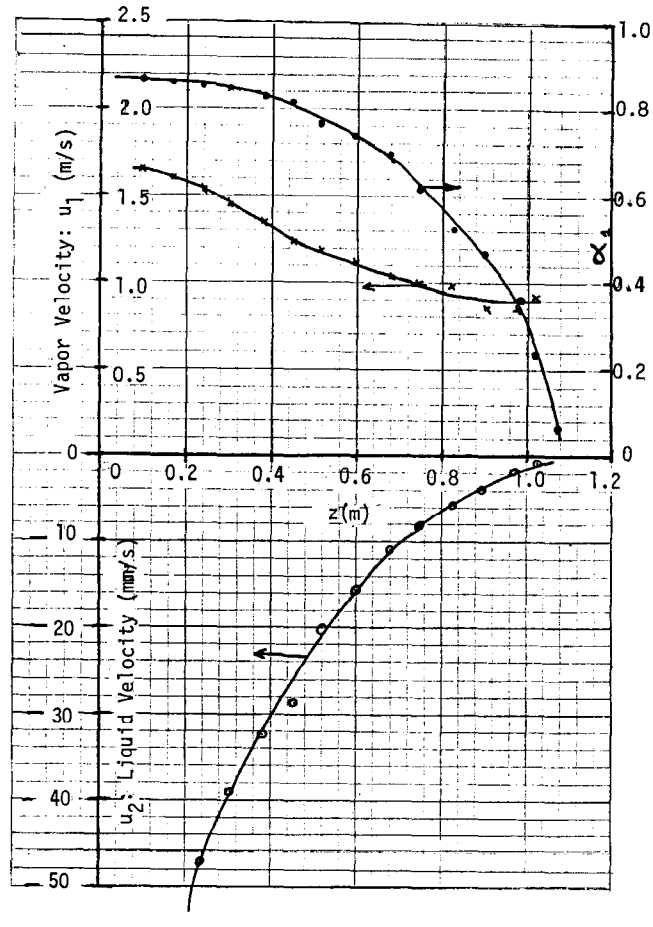

Figure 19 Data on liquid and vapor velocities and void fraction during reflux condensation near the flooding point.

downward at the top. This is at variance with the measurements. The same result is found in all the experiments we have done in this regime [see Nguyen and Banerjee (1985)]. Clearly, something is wrong with the model!

The reasons for this curious behaviour in wall shear stress may be explained qualitatively as follows: Consider the flow to be oscillatory, with large waves travelling upwards at velocities close to that of the vapor, and relatively slow downflow in the liquid film between waves. The shear stress under the waves is high because of the high-velocity upflow, whereas the wall shear stress in the draining film is low. However, as the vapor condenses, its velocity is reduced, and the wave velocity is also reduced. As a consequence, the shear stress at some point goes to zero, because the component due to upflow in the waves is exactly balanced by downflow in the film. Below this point, the wave velocity is high enough to give a negative shear stress, whereas above this point shear stress is positive. The data can be explained more quantitatively if observed values of wave frequency and velocity are used, together with appropriate velocity gradients at the wall in the wave and draining film regions.

The question, however, is to determine whether the multifield model can be modified to incorporate such phenomena. The correlations required for wall and interfacial shear stress in the slug / churn would clearly have to be quite different from (40).

A method to deal with problems of this nature has not yet been developed. One possibility is to divide the liquid flow into 2 fields – a wave or slug field and a film field. The momentum interactions in these fields with the gas / vapor and the wall would be quite different. At present, there appears to be no information which can be obtained from the model about the division of liquid between these fields. Information on disturbance length, amplitude, and frequency is needed to proceed further, and it appears this has to be supplied to the model on the basis of experiments. However, we speculate that careful stability analysis of the model could lead to disturbance frequencies and lengths. Almost certainly this analysis would have to take some non-linear effects into account.

In summary, then, the multifield model successfully captures many subtle phenomena in 2-phase flows, where oscillations are small compared to the mean flow. However, in regimes where the oscillations are

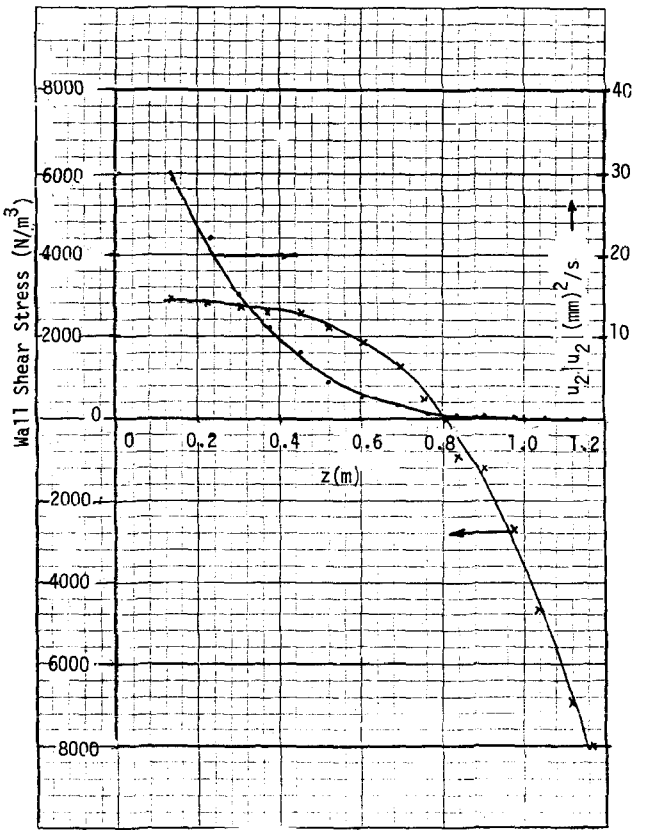

Figure 20 Data on wall shear stress and liquid velocity during reflux condensation showing that the wall shear stress is not proportional to the square of the mean velocity.

much larger, the model is more difficult to apply. The difficulty lies in determining the correct closure relationships. If the present framework for closure relationships is used, then the limitations are clear – experimental measurements on wall and interface momentum interactions cannot be predicted for intermittent flows.

Acknowledgements

This paper was originally presented at the Second International Conference on Simulation Methods in Nuclear Engineering, Montreal, 14–16 October 1986.

References

1. *Agee LJ, Banerjee S, Duffey RB, Hughes ED.* Some aspects of two fluid models and their numerical solutions. Second OECD Specialists Meeting on Transient Two Phase Flow 1978; 1: 27–58.
2. *Ahmed R, Banerjee S.* Finite amplitude waves in stratified two-phase flow: transition to slug flow. AIChE J 1985; 31: 1480–7.
3. *Ardron KH.* One-dimensional two-fluid equations for horizontal stratified two-phase flow. Int J Multiphase Flow 1980; 6: 295–304.
4. *Banerjee S, Chan AMC.* Separated flow model. I. Analysis of the averaged and local instantaneous formulations. Int J Multiphase Flow 1980; 6: 1–24.
5. *Banerjee S.* Separated flow models. II. Higher order dispersion effects in the averaged formulation. Int J Multiphase Flow 1980; 6: 241–8.
6. *Banerjee S.* Closure relationships and constitutive equations. Lecture presented at Two-Phase Flow Short Course, ETH-Zurich, March 1985.
7. *Bernier RJ.* Unsteady two-phase flow instrumentation and measurement. Cal Tech, Engr Appl Sci Div, Report No. E200.4, 1981.
8. *Bird RB, Stewart WE, Lightfoot E.* Transport phenomena. John Wiley, 1960: 191–2, 220–1.
9. *Boure JA.* On a unified presentation of the non-equilibrium two phase flow models in non-equilibrium two phase flows. *In:* ASME Symposium Volume, Eds. Lahey RT, Jr, Wallis GB. New York: ASME, 1975.
10. *Chan AMC, Banerjee S.* Refilling and rewetting of a hot horizontal tube. Part I. Experiments. J Heat Transfer 1981a; 103: 281–6.
11. *Chan AMC, Banerjee S.* Refilling and rewetting of a hot horizontal tube. Part II. Structure of a two-fluid model. J Heat Transfer 1981b; 103: 287–92.
12. *Chan AMC, Banerjee S.* Refilling and rewetting of a hot horizontal tube. Part III. Application of a two-fluid model to analyze rewetting. J Heat Transfer 1981c; 103: 653–9.
13. *De Jarlais G.* An experimental study of inverted annular flow hydrodynamics utilizing an adiabatic simulation. NUREG / CR-3339, 1983.
14. *Delhaye DA.* Contribution à l'étude des écoulements diphasiques eau-air et eau-vapeur. Ph.D. Thesis, University of Grenoble, 1970.
15. *Delhaye JM, Achard JL.* On the averaging operators introduced in two phase flow modeling. Proc CSNI Specialists Meeting in Transient Two Phase Flow. Eds. Banerjee S, Weaver KR. Toronto, Aug. 3–4, 1976.
16. *Drew DA.* Average field equations for two-phase media. Studies in Applied Mathematics 1971; 1.
17. *Drew DA, Cheng L, Lahey RT, Jr.* Analysis of virtual mass effects in two phase flow. Int J Multiphase Flow 1979; 5: 233–42.
18. *Drew DA, Lahey RT, Jr.* Application of general constitutive principles to the derivation of multidimensional two phase flow equations. Int J Multiphase Flow 1979; 5: 243–64.
19. *Drew DA.* Mathematical modelling of two phase flow. Ann Rev Fluid Mech 1983; 15: 261–91.
20. *Haas FC.* Stability of droplets suddenly exposed to a high velocity gas stream. AIChE J 1976; 10: 920–4.
21. *Hanson AR, Domich EG, Adams HS.* Shock tube investigation of the breakup of drops by air blasts. Physics of Fluids 1963; 6: 1070–80.
22. *Hinze JO.* Critical speeds and sites of liquid globules. Appl Sci Res 1948; A1: 273–88.
23. *Hinze JO.* Fundamentals of the hydrodynamic mechanism of splitting in dispersion process. AIChE J 1953; 1: 289–95.
24. *Hughes ED, Lyczkowski RW, McFadden Niederauer GF.* An evaluation of state of the art two velocity two phase flow

models and their applicability to nuclear reactor transient analysis. EPRI Report NP143, 1976; 1, 2, 3.
25. *Ishii M.* Thermally induced flow instabilities in two-phase mixtures in thermal equilibrium. Ph.D. Thesis, Georgia Institute of Technology, 1971.
26. *Ishii M.* Thermo-fluid dynamic theory of two phase flow. Paris: Byrolles, 1975.
27. *Kataoka I, Ishii M, Mishima K.* Generation and size distribution of droplets in annular two-phase flow. ASME J Fluids Engr 1983; 105: 230–8.
28. *Kawaji M, Banerjee S.* Application of a two-field model to reflooding of a hot vertical tube. I. Model structure and interfacial phenomena. J Heat Transfer 1987; 109: 204–11.
29. *Kocamutafaogullari G.* Thermo-fluid dynamics of separated two-phase flow. Ph.D. Thesis, Georgia Institute of Technology, 1971.
30. *Lahey RT, Jr, Cheng L, Drew D, Flaherty J.* The effect of virtual mass on the numerical stability of accelerating two phase flow. Int J Multiphase Flow 1980; 6: 281–94.
31. *Lane WR.* Shatter of drops in streams of air. Ind Eng Chem 1951; 43: 1312–7.
32. *Lyckowski RW.* Theoretical bases of the drift flux field equations and vapor drift velocity. Proc 6th Int Heat Transfer Conf Washington: Hemisphere Press, 1978; 1: 339–44.
33. *Nguyen Q, Banerjee S.* Interfacial heat and momentum transfer for condensation in vertical tubes. Paper presented at AIChE annual meeting, Chicago, 1985.
34. *Nigmatulin RI.* Averaging in mathematical modeling of heterogeneous and dispersed mixtures. Paper presented at International Center for Heat and Mass Transfer Symposium, Yugoslavia, 1978.
35. *Nigmatulin RI.* Spatial averaging in the mechanics of heterogeneous and dispersed systems. Int J Multiphase Flow 1979; 5: 353–85.
36. *Panton RJ.* Flow properties for the continuum viewpoint of a nonequilibrium gas particle mixture. J Fluid Mech 1978; 31: 273–303.
37. *Pauchon C, Banerjee S.* Interphase momentum interaction effects in the averaged multifield model. I. Void propagation in bubbly flows. Int J Multiphase Flow 1986; 12: 559–73.
38. *Ramshaw JD, Trapp JA.* Characteristics, stability, and short wavelength phenomena in two phase flow equation systems. Nuc Sci and Engineering 1978; 66: 93–102.
39. *Ransom VH,* et al. RELAP5/MOD2 code manual. Vol. I. Code structure, system models and solution methods. EGG-SAAM-6377, 1984.
40. *Rousseau JC, Ferch RL.* A note on two-phase separated flow models. Int J Multiphase Flow 1979; 5: 489–93.
41. *Ryan RT.* The behavior of large, low-surface-tension water drops falling at terminal velocity in air. J Appl Meteor 1976; 15: 157–65.
42. *Sleicher CA.* Maximum stable drop size in turbulent flows. AIChE J 1967; 8: 471–7.
43. TRAC-PD2, an advanced best estimate computer program for PWR loss of coolant accident analysis. Los Alamos National Lab. Rept. LA-8709-MS (NUREG/CR-2054), 1981.
44. *Vernier P, Delhaye JM.* General two phase flow equation applied to the thermo-hydrodynamics of boiling water nuclear reactors. Energie Primaire 1968; 4.
45. *Wallis GB.* The terminal speed of single drops or bubbles in an infinite medium. Int J Multiphase Flow 1974; 1: 491–511.
46. *Yadigaroglu G, Lahey RT.* On the various forms of the conservation equations in two phase flow. Int J Multiphase Flow 1976; 2: 477–94.